11-6-2017

Ir d-band derived superconductivity in the lanthanum-iridium system LaIr3

Neel Haldolaarachchige
Rowan University

Leslie Schoop
Princeton University

Mojammel A. Khan
Louisiana State University

Wenxuan Huang
Massachusetts Institute of Technology

Huiwen Ji
Princeton University

See next page for additional authors

Recommended Citation

Haldolaarachchige, N., Schoop, L., Khan, M., Huang, W., Ji, H., Hettiarachchilage, K., & Young, D. (2017). Ir d-band derived superconductivity in the lanthanum-iridium system LaIr3. *Journal of Physics Condensed Matter, 29* (47) https://doi.org/10.1088/1361-648X/aa90a8

Ir *d*-band Derived Superconductivity in the Lanthanum-Iridium System $LaIr_3$

Neel Haldolaarachchige,[1,2] Leslie Schoop,[3] Mojammel A. Khan,[4]
Wenxuan Huang,[5] Huiwen Ji,[3] Kalani Hettiarachchilage,[2,6] and David P. Young[4]

[1] *Department of Physics and Astronomy, Rowan University, Glassboro, NJ08028, USA*
[2] *Department of Physics and Engineering, College of Staten Island, The City University of New York, NY10314, USA*
[3] *Department of Chemistry, Princeton University, Princeton, NJ08540, USA*
[4] *Department of Physics and Astronomy, Louisiana State University, Baton Rouge, LA70803, USA*
[5] *Department of Mat. Sci. and Eng., Massachusetts Institute of Technology, Cambridge, MA 02142, USA*
[6] *Department of Physics, The College of New Jersey, Ewing, NJ08618, USA*

The electronic properties of the heavy metal superconductor $LaIr_3$ are reported. The estimated superconducting parameters obtained from physical properties measurements indicate that $LaIr_3$ is a BCS-type superconductor. Electronic band structure calculations show that Ir *d*-states dominate the Fermi level. A comparison of electronic band structures of $LaIr_3$ and $LaRh_3$ shows that the Ir-compound has a strong spin-orbit-coupling effect, which creates a complex Fermi surface.

I. INTRODUCTION

The combination of rare earth and main group transition metal elements can produce compounds with complex, technologically important, and scientifically interesting physical properties. Compounds with $5d$ transition metals show electron correlations and spin-orbit interactions that create interesting electronic properties, such as superconductivity. [1] Only a few Ir compounds are known to display superconductivity and most of their electronic properties are due to the rare earth elements rather than Ir. [2–5] There are, however, a few examples, such as $CaIr_2$, IrGe and $Mg_{10}Ir_{19}B_{16}$, where the superconductivity is derived from Ir-d states at the Fermi surface. [6–8] Evens so, there is no simple example of a lanthanide-iridium superconductor whose properties are dominated by Ir-d bands at the Fermi level and strong spin-orbit-coupling.

Here we report the synthesis, experimental superconducting parameters of $LaIr_3$ and $LaIr_{2.8}$ and the calculated electronic band structure of $LaIr_3$ and $LaRh_3$. The existence of superconductivity in $LaIr_3$ has been reported earlier, but besides its superconducting transition temperature T_c, no further characterization is available, except one report on a doping study. [9, 10] $LaIr_3$ is unusual among the lanthanide superconductors, because it contains $5d$ electrons with no magnetic rare earth ions present. The reported T_c of $LaIr_3$ is, however, comparable to most Ce $4f$ based superconductors. [12, 13] Still, the superconducting transition temperature of $LaIr_3$ is much lower than those of the alkaline-based Ir superconductors such as $CaIr_2$. [8] The isostrucutral compound $LaRh_3$ was also reported to be superconducting with a slightly lower than that of $LaIr_3$. [14]

II. EXPERIMENT AND CALCULATION

Polycrystalline samples of $LaIr_3$ were prepared with ultra pure (5N, 99.999%) elemental La and Ir by arc melting. The arc-melted button was sealed inside a quartz tube under vacuum. The tube was then heated (heating rate is 180 ^{0}C per hour) to 1000 ^{0}C and held at that temperature for about 24 hrs. The quartz tubes with the samples inside were then removed from the furnace and quenched in water. Powder X-ray diffraction (PXRD) were performed to check the phase purity and cell parameters of the samples at room temperature on a Bruker D8 FOCUS diffractometer (Cu K_α). MAUD program was used for detailed Rietveld analysis. [15] The X-ray investigation confirmed that the sample was a single phase with a rhombohedral crystal symmetry with the space group 166 (R -3 m). [11] A small amount of elemental Ir was detected as an impurity, but this dose not effect on the observed physical properties of the sample (Ir metal superconduct at very low temperature 0.14K). [16] Energy Dispersive Spectroscopy (EDS) is used for further investigation of the sample purity by using FEI XL30 FEG-SEM system equipped with EVEX EDS, and confirmed the stoichiometry (ratio of La:Ir) of the sample as 1:3.

Standard four-probe method was used to measure electrical resistance with an excitation current of 10 mA; small diameter Pt wires were attached to the sample using a conductive epoxy (Epotek H20E). Quantum Design Physical Property Measurement System (PPMS) was used to collect the data from 300K - 2K and in magnetic fields up to 5 T (Tesla). Time-relaxation method was used to measure specific heat between 2 K and 50 K in the PPMS, using zero field and 5 T applied magnetic field. The magnetic susceptibility was measured in a DC field of 10 Oe; the sample was cooled down to 1.8 K in zero-field, the magnetic field was then applied, and the sample magnetization was measured on heating to 4 K [zero-field-cooled (ZFC)], and then on cooling to 1.8 K [field-cooled (FC)] in the PPMS.

Density functional theory (DFT) based computational method was used to calculate the electronic structure with the WIEN2K code with a full-potential linearized augmented plane-wave and local orbitals [FP-LAPW

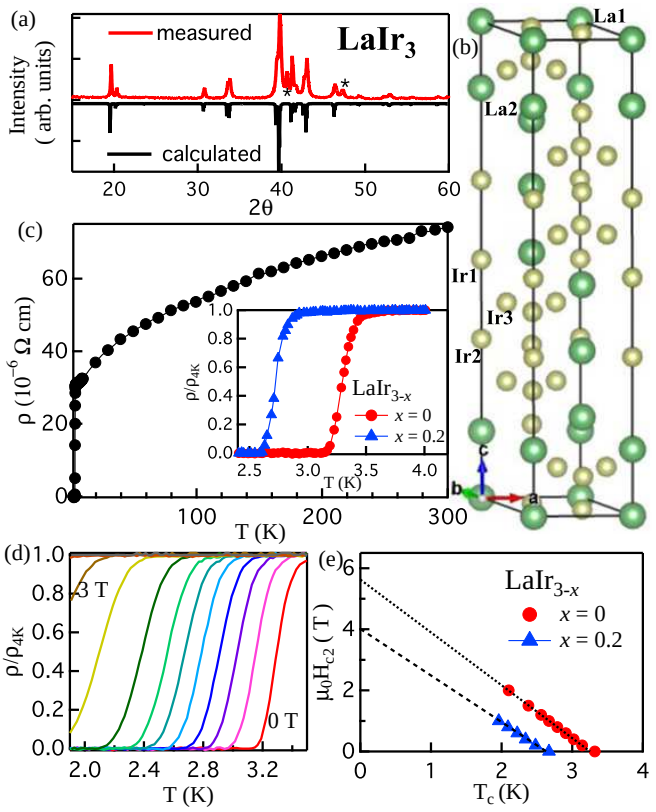

FIG. 1. (Color online) Analysis of the powder X-ray diffraction (PXRD) and resistivity of $LaIr_3$. (a) Measured powder X-ray diffraction and calculated XRD patterns of $LaIr_3$. (b) 3D crystal structure of rhombohedral $LaIr_3$. (c) Resistivity at zero applied field. Inset of (c) shows normalized resistance at low temperature of $LaIr_3$ and $LaIr_{2.8}$. (d) Normalized resistance of $LaIr_3$ with increasing applied magnetic field from 0 - 3 T. (e) The upper critical field as a function of temperature.

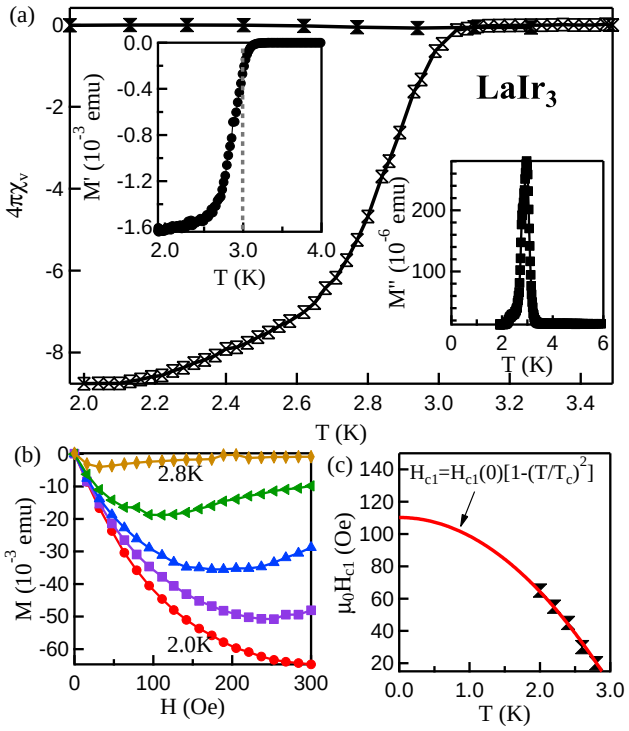

FIG. 2. (Color online) Analysis of magnetization of $LaIr_3$. (a) The ZFC and FC DC magnetization of $LaIr_3$. Inset of (a) shows the AC magnetization. (b) DC magnetization (M vs. H curves) at different temperatures from 2K to 2.8K, below the superconducting temperature T_c. (c) The lower critical field as a function of temperature.

+ lo] basis [18–21] together with the PBE parameterization [22] of the GGA, with and without spin orbit coupling (SOC). The plane-wave cutoff parameter $R_{MT}K_{MAX}$ was set to 7, and the Brillouin zone was sampled by 20,000 k points. Convergence was confirmed by increasing both $R_{MT}K_{MAX}$ and the number of k points until no change in the total energy was observed. Program Crysden was used to plot the Fermi surface for the calculated band structure.

III. RESULTS AND DISCUSSION

Fig. 1.(a) shows measured powder X-ray diffraction (PXRD) (upper line) and calculated PXRD pattern (lower line) of polycrystalline $LaIr_3$. Two pattern match perfectly, which confirms the rhombohedral crystal structure with space group number 166 (R -3 m). However, very small amount of elemental Ir impurity (asterisk marks on the Fig. 1.(a)) detected on the PXRD and this does not have any effect on observed physical properties of $LaIr_3$ because, elemental Ir superconduct only at very low temperature (0.14 K). [16, 17] Fig. 1.(b) shows 3D crystal structure of $LaIr_3$. Large green symbols represents La atoms and small yellow symbols represents Ir atoms. Rhombohedral unit cell contains two distinct La atoms (La1 and La2) and three distinct Ir atoms (Ir1, Ir2 and Ir3). Fig. 1.(c) shows the temperature dependent resistivity of $LaIr_3$ from 300K to 2K. The normal state resistivity shows poor metallic behavior $\left(\frac{d\rho}{dT} > 0\right)$ of the polycrystalline sample, with a very low room temperature resistivity. Inset of Fig. 1.(c) shows a clear superconducting transition (T_c^{onset}) of $LaIr_3$ at 3.3 K and a slightly lower T_c^{onset} for $LaIr_{2.8}$ at 2.75 K. We have tested both Ir and La off-stoichiometric effects on the superconducting T_c of this material. La deficiency did not show a strong effect, however Ir deficiency did affect T_c significantly. This demonstrates the strong effect of Ir bands around the Fermi level, which is consistent with the band structure calculation studies later discussed in this manuscript. The low-temperature resistivity (above T_c, from 4 K - 25 K) data can be described by a power law $\rho = \rho_0 + AT^n$ with $n = 2$, which follows Fermi liquid behavior with the residual resistivity $\rho_0 = 30\ \mu\Omega cm$, and the coefficient $A = 2.35 \times 10^{-8}\ \frac{\Omega cm}{K^2}$.

The high temperature (above 25 K) data significantly deviates from Fermi Liquid behavior and show a tendency to saturate at higher temperatures. This behavior can be related to the Ioffe-Regel limit [24], when the charge carrier mean free path is comparable to the interatomic spacing and/or to two-band conductivity. [25] Similar behavior was observed for other Ir-based superconductors, such as $CaIr_2$. [8] Extracted value of A is related to the degree of electron correlations in a system, which suggests that $LaIr_3$ is a weakly correlated electron system. [26]

Magnetoresistance data for $LaIr_3$ is shown in Fig. 1(d). Increasing magnetic field shows the width of the superconducting transition increases slightly. The Werthamer-Helfand-Hohenberg (WHH) expression is used to estimate the orbital upper critical field by using the 50% normal state resistivity point as the transition temperature, $\mu_0 H_{c2}(0) = -0.693\ T_c \frac{dH_{c2}}{dT}|_{T=T_c}$. [23] Fig. 1(e) between $\mu_0 H_{c2}$ and T_c shows linear relationship. $\mu_0 H_{c2}(0) = 3.84$ T is calculated by using slope of the graph and the value of $\mu_0 H_{c2}(0)$ is smaller than the weak-coupling Pauli-paramagnetic limit $\mu_0 H^{Pauli} = 1.82\ T_c = 6.10$ T for $LaIr_3$. Empirical formula $H_{c2}(T) = H_{c2}(0)\left[1 - \left(\frac{T}{T_c}\right)^{\frac{3}{2}}\right]^{\frac{3}{2}}$ is also used to calculate the orbital upper critical field and the calculated value agrees well with the value of WHH method. Both of the above formulas (WHH expression and the empirical formula) are widely used to calculate $\mu_0 H_{c2}(0)$ for a variety of intermetallic and oxide superconductors. [27–34] Upper critical field $\mu_0 H_{c2}(0)$ and $\xi(0) = \sqrt{\Phi_0/2\pi H_{c2}(0)} = 92.59$ Å are used to calculate the Ginzburg-Landau coherence length, where $\Phi_0 = \frac{hc}{2e}$ is the magnetic flux quantum. [35, 36] Calculated value is comparable to the recently reported Ir based Laves phase superconductor $CaIr_2$, which further suggests the effect of Ir sub-lattice on both compounds. [8]

Fig. 2 shows analysis of the magnetization of $LaIr_3$. Zero-field-cooled (ZFC-shielding) and field-cooled (FC-Meissner) data in Fig. 2(a) confirms the superconducting shielding fraction. The bulk superconducting transition $T_c^{onset} = 3.1$ K is extracted from the graph. Resistivity and susceptibility measurements show similar values of T_c, which indicates the polycrystalline sample is homogeneous. Inset of Fig. 2(a) further verifies the superconducting $T_c = 3.1$ K by AC susceptibility. Upper left inset shows real part of AC-susceptibility with $T_c^{onset} = 3.1$ K and lower right inset shows imaginary part of AC-susceptibility with similar T_c. The magnetization as a function of magnetic field over a range of temperatures below T_c is shown in Fig. 2(b). To analyze the lower critical field, T_c for each magnetic field was selected by using 2.5% deviation from the full shielding effect. Fig. 2(c) shows $\mu_0 H_{c1}$ as a function of T_c. $H_{c1}(T) = H_{c1}(0)\left[1 - \left(\frac{T}{T_c}\right)^2\right]$ is used to analyze the lower critical field behavior and the $\mu_0 H_{c1}$ data are well described with the above equation. $\mu_0 H_{c1}(0)$=110.24 Oe

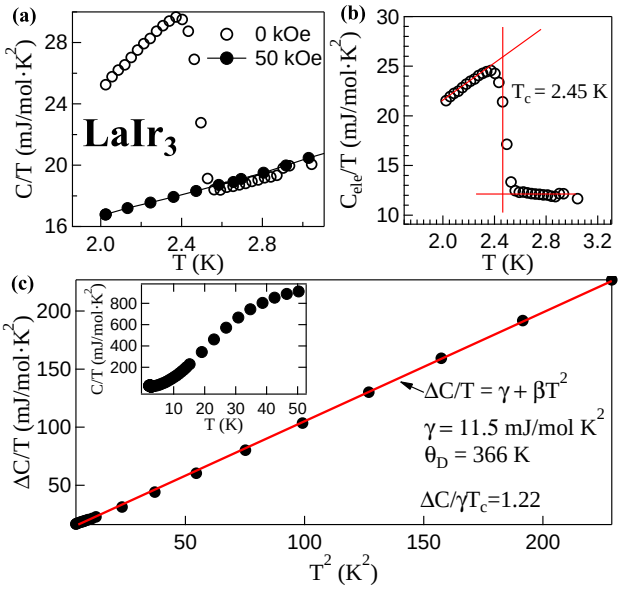

FIG. 3. (Color online) Analysis of heat capacity of $LaIr_3$. (a) Heat capacity at zero (open symbol) and 5 T (Tesla) (closed symbol) applied field. (b) The electronic heat capacity jump, which can be used to extract T_c by using the equal-area construction method. (c) The 5 T heat capacity data. The solid line shows the fit with equation $\frac{C}{T} = \gamma + \beta T^2$. The upper left inset shows the zero-field heat capacity as a function of temperature.

TABLE I. Superconducting Parameters of $LaIr_3$.

Parameter	Units	$LaIr_3$
T_c	K	3.32
ρ_0	$m\Omega cm$	3.05×10^{-2}
$\frac{dH_{c2}}{dT}\|_{T=T_c}$	$T\ K^{-1}$	-1.67
$\mu_0 H_{c1}(0)$	Oe	110.24
$\mu_0 H_{c2}(0)$	T	3.84
$\mu_0 H^{Pauli}$	T	6.11
$\mu_0 H(0)$	T	0.0175
$\xi(0)$	Å	92.59
$\lambda(0)$	Å	960
$\kappa(0)$	Å	10.37
$\gamma(0)$	$\frac{mJ}{mol\ K^2}$	11.5
$\frac{\Delta C}{\gamma T_c}$		1.22
Θ_D	K	366
λ_{ep}		0.57
$N(E_F)$	$\frac{eV}{f.u.}$	0.72

is extracted by using least squares fit, which is much smaller than that of the cubic Laves phase $CaIr_2$. [8]

Fig. 3 shows the analysis of specific heat (C) measurements. Specific heat jump at the thermodynamic transition is shown in Fig. 3(a). Applied magnetic field of 5T is fully suppressed the heat capacity jump. The super-

conducting transition temperature of $T_c = 2.45$ K is extracted by the standard equal area construction method (see Fig. 3(b)). It is not very uncommon to see lower critical temperature from specific heat measurement compare to resistivity measurement, as heat capacity is a bulk measurement, and resistivity and susceptibility can be sensitive to surface super currents that appear at higher temperature. The low temperature normal state specific heat is well fit with the Debye model. The solid line in Fig. 3(c) shows the fitting; the electronic specific heat coefficient $\gamma = 11.5\frac{mJ}{mol\ K^2}$, and the phonon/lattice contribution $\beta = 0.906\frac{mJ}{mol\ K^4}$ is extracted from the fit. The value of γ obtained is comparable to the cubic Laves phase superconductor $CaIr_2$, [8] and some other Ir-based heavy element superconductors, which further suggests the common effect of Ir-sub-lattice on many Ir based superconducting materials. [3, 13] Also, low gamma value on $LaIr_3$ may be due to the absence of f-orbitals near Fermi level and further details can be found on band structure figures later on this manuscript.

Strength of the electron-phonon coupling is estimated with $\frac{\Delta C}{\gamma T_c}$. [37] Which is calculated as 1.22 (specific heat jump $\frac{\Delta C}{T_c} = 14\ \frac{mJ}{mol\ K^2}$). Calculated value is lower than 1.43 for a conventional BCS superconductor and it suggests that $LaIr_3$ is a weakly electron−phonon coupled superconductor. Debye temperature Θ_D is calculated by using $\beta = nN_A\frac{12}{5}\pi^4 R\Theta_D^{-3}$, where $R = 8.314\ \frac{J}{mol\ K}$, n is the number of atoms per formula unit, and N_A is Avogadro's number. The calculated Debye temperature for $LaIr_3$ is 366 K, which is slightly higher than that of $CaIr_2$. [8] McMillan formula $\lambda_{ep} = \frac{1.04+\mu^* ln\frac{\Theta_D}{1.45T_c}}{(1-0.62\mu^*)ln\frac{\Theta_D}{1.45T_c}-1.04}$ is generally used to calculate the strength of the electron-phonon coupling. [38, 39] Dimensionless electron-phonon coupling constant λ_{ep} is within the McMillan's model, which, in Eliashberg theory, is related to the phonon spectrum and the density of states. Attractive interaction represents by the parameter λ_{ep}, while the screened Coulomb repulsion represents by the second parameter μ^*. The electron-phonon coupling constant (λ_{ep}) for $LaIr_3$ is calculated as 0.57 by using the Debye temperature Θ_D, critical temperature T_c, and making the common assumption that $\mu^* = 0.15$, [38] Weak electron-phonon coupling behavior from $\lambda_{ep} = 0.57$ agrees well with $\frac{\Delta C}{\gamma T_c} = 1.22$.

The measured magnetic susceptibility of $LaIr_3$ at 10 K is $\chi = 1.44 \times 10^{-6}\frac{emu\ m^3}{mol\ f.u.}$, which can be considered as a spin susceptibility. This allows for an estimate of the Wilson ratio $R_W = \frac{\pi^2 k_B^2 \chi_{spin}}{3\mu_B^2 \gamma} = 0.21$, which is smaller than that of the free electron value of 1. Also, the coefficient of the quadratic resistivity term can be normalized with the effective mass term from the heat capacity, which results in the Kadowaki-Woods ratio $\frac{A}{\gamma^2}$. This ratio is found to be 0.39 a_0, where $a_0 = 10^{-5}\frac{m\Omega\ cm}{(mJ/mol\ K)^2}$. R_W and $\frac{A}{\gamma^2}$ both indicate that $LaIr_3$ is a weakly-correlated electron system. [40–42]

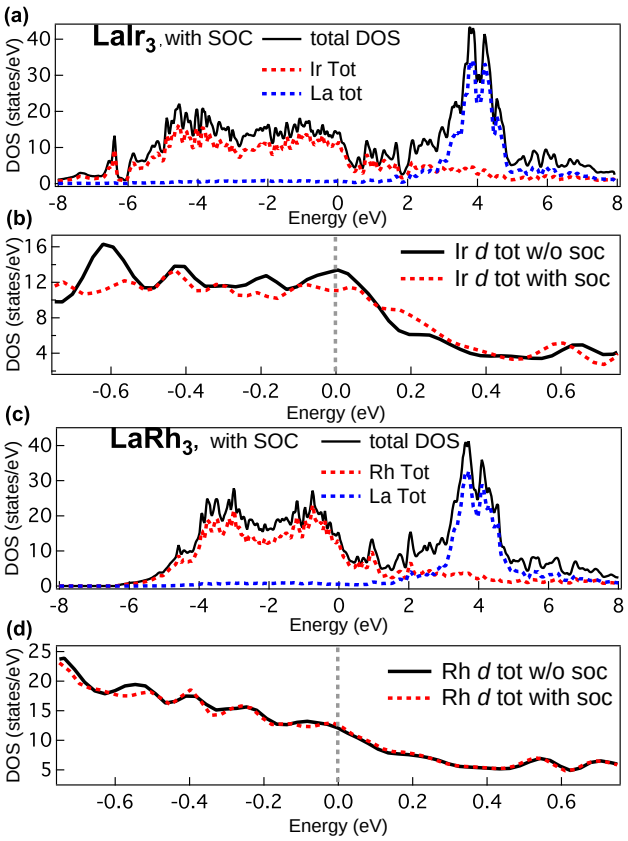

FIG. 4. (Color online) The density of states of $LaIr_3$ and $LaRh_3$. (a) The total DOS of $LaIr_3$, as well as the contributions of La and Ir states respectively. Spin-orbit coupling (SOC) is included. (b) Ir d-band DOS with and with-out SOC. (c) The total DOS of $LaRh_3$, as well as the contributions of La and Rh states respectively. Spin-orbit coupling (SOC) is included. (d) Rh d-band DOS with and with-out SOC.

All the measured and calculated superconducting parameters of $LaIr_3$ are summarized and presented in Table. I.

Fig. 4 shows the analysis of the density of states (DOS) of isostructural $LaIr_3$ and $LaRh_3$. It can be clearly observed that the Ir states (Fig. 4(a)) and Rh states (Fig. 4(c)) dominate near the Fermi level, respectively. The contribution of La states is almost negligible at the Fermi level in both systems. Detailed analysis of the DOS calculated with and without SOC shows that it is affecting the $LaIr_3$ system significantly, but not $LaRh_3$. To further investigate the effect of SOC, the partial DOS of both systems is plotted in Fig. 4(b) and (d). It can be clearly observed that the Ir-d states and Rh-d states are dominant near the Fermi level. However, the Ir compound clearly shows a stronger SOC effect, while there is no such effect in the Rh system. This is similar to other Ir based superconducting systems such as $CaIr_2$. [8] The partial DOS analysis shows that the total DOS is dominated by the contributions from the Ir sublattice, and

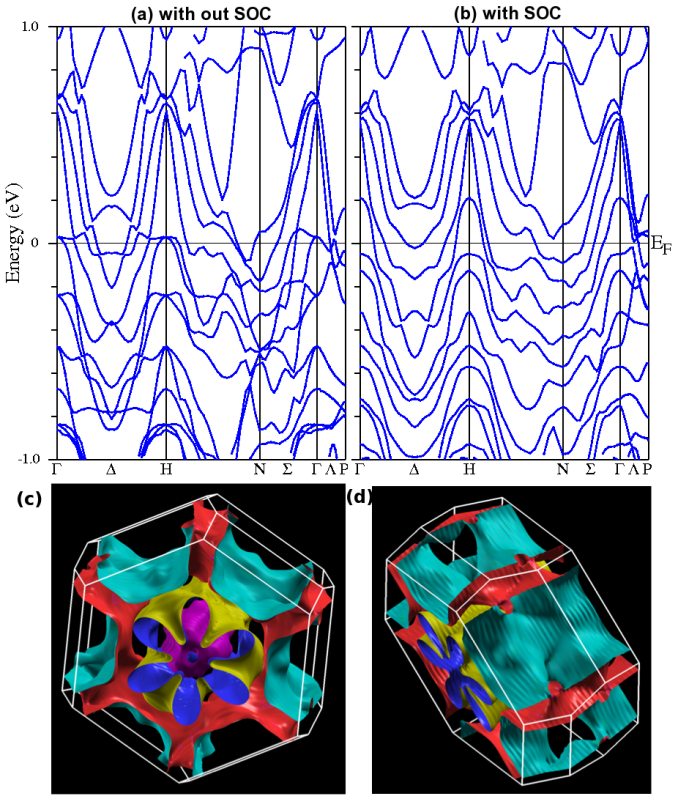

FIG. 5. (Color online) Electronic band structure of $LaIr_3$. (a) Band-structure with-out SOC and (b) band-structure with SOC. Complex Fermi surface shows on (c) and (d) for merged bands.

that the contribution from the La atoms near the Fermi level is almost negligible. Given the radical change in the Fermi surface (see Fig. 5) due to the spin orbit coupling compared to the hypothetical case where no spin orbit coupling is present, one can speculate that SOC has an effect on the superconducting properties of $LaIr_3$. This is further strengthened by the fact that T_c is lower in the isostructural Rh analog, where SOC is negligible. [14] $LaIr_3$ is thus a rare-example of a lanthanide superconductor that is superconducting due the effect of $5d$ electrons.

Fig. 5 shows the calculated band structure of $LaIr_3$. The SOC effect can be clearly observed near the Fermi level of Fig. 5(b) and significant differences can be observed between the Fig. 5(a) without SOC and Fig. 5(b) with SOC. Cubic laves phase superconductor $CaIr_2$ [8] also shows the similar behavior. 3D metallic nature is observed from the band structure of $LaIr_3$; several bands with large dispersion cross the Fermi level. Ir $5d$-orbitals are the only bands visible near Fermi level. This suggests that the superconducting electrons are strongly effected by the Ir sub-lattice of $LaIr_3$. Calculated complex Fermi surface (See Fig. 5(c) and (d)) is a result of many bands crossing the Fermi energy.

$LaIr_3$ is an rare-earth based superconductor with the presence of f-orbitals. However, this study suggests that superconductivity of this system is derived by $5d$-orbitals of Ir-sublattice and there is no any effect from La f-orbitals. And also, this study further suggests that strong effect of SOC on Ir-$5d$ bands, which is very commonly found on many other Ir based superconductors. [2–6, 8] To investigate further the role of rare-earth elements and SOC effect from Ir $5d$ bands, other rhombohedral structure type RIr_3 materials with R-lanthanides (with $4f$) [10] will be an excellent playground. Specially materials with partially filled $4f$ orbitals, such as Pr, Ce, *etc.,* will show magnetism effect and possible superconductivity. Also, it may be very interesting and important to see the real band structure of these RIr_3 materials by using angle resolved photoelectron spectroscopy (ARPES). And specially $CeIr_3$ [10] is reported to be a superconductor but there is no detail studies reported so far. We think that $CeIr_3$ and doped series of $LaIr_3$ to $CeIr_3$ will be an excellent study to further investigate, which will possibly show unusual physical properties due to the effect of magnetic rare earth element of Ce with f orbitals and possible strong correlations effects of Ce $4f$ and Ir $5d$ bands.

IV. CONCLUSION

Here, we have reported the synthesis and characterization of $LaIr_3$, which displays superconductivity below $T_c = 3.3K$. $LaIr_3$ is a superconductor where the bands near the Fermi surface are dominated by Ir $5d$ states that are strongly affected by SOC. Thus, it is one of the few examples of a lanthanide-based superconductor where $5d$ electrons play the dominate role in the superconductivity. The superconducting parameters obtained from physical properties measurements of $LaIr_3$ suggest that it is a weakly-coupled BCS-type superconductor. These results motivate future work focused on exploring intermetallic Ir-based superconductors that form in noncentrosymmetric structure types. Strong SOC in these systems would then be antisymmetric, which often leads to exotic and unconventional superconductivity.

V. ACKNOWLEDGMENTS

DPY acknowledges support from the NSF through Grant No. DMR-1306392.

[1] S. M. Disseler, Chetan Dhital, A. Amato, S. R. Giblin, Clarina de la Cruz, Stephen D. Wilson, and M. J. Graf1, Phy. Rev. B **86**, 014428 (2012).

[2] R. Movshovich, M. Jaime, J. D. Thompson, C. Petrovic, Z. Fisk, P. G. Pagliuso, and J. L. Sarrao, Phy. Rev. Lett. **86**, 5152, (2007).

[3] Daigorou Hirai, Mazhar N. Ali, and Robert J. Cava, J. Phys. Soc. Jpn. **82** 124701 (2013).

[4] Fabian von Rohr, Huixia Luo, Ni Ni, Michael Worle, and Robert J. Cava, Phy. Rev. B **89**, 224504 (2014).

[5] F. Honda, I. Bonalde, S. Yoshiuchi, Y. Hirose, T. Nakamura, K. Shimizu, R. Settai, and Y. Onuki, Physica C Superconductivity **470**, 543 (2010).

[6] Daigorou Hirai, Rui Kawakami, Oxana V. Magdysyuk, Robert E. Dinnebier, Alexander Yaresko, and Hidenori Takagi, Journal of the Physical Society of Japan **83**, 103703 (2014).

[7] T. Klimczuk, F. Ronning, V. Sidorov, R. J. Cava and J. D. Thompson, Phy. Rev. Lett. **99**, 257004 (2007).

[8] Neel Haldolaarachchige, Quinn Gibson, Leslie M Schoop, Huixia Luo, R. J Cava, Journal of Physics: Condensed Matter **27**, 18, 185701 (2015).

[9] M. Hakimi and J. G. Huber, Physica **135B**, 434-437 (1985).

[10] J. G. Huber, Physica **163**, 213-229 (1990).

[11] Akad, Nauk Ukraiskoi, Metallofizika **52**, p121-p123 (1974).

[12] A. D. Huxley, C. Paulsen, O. Laborde, J. L. Tholence, D. Sanchez, A. Junod, R. Calemczuk, J. Phys. Condens. Matter **5**, 7709 (1993).

[13] Hitoshi Sugawara, Hideyuki Sato, Tsuyoshi Yamazaki, Noriaki Kimura, Rikio Settai, and Yoshichika nuke, J. Phys. Soc. Jpn. **64**, 4849-4855 (1995).

[14] T. H. GeballIe, B. T. Matthias, V. B. Compton, E. Corenzwit, G. W. Hull, and D. Longinotti, Phys. Rev. **137**, A119 (1965).

[15] L. Lutterotti, S. Matthies, H. R. Wenk - IUCr: Newsletter of the CPD, 1999

[16] R. A. Hein, J. W. Gibson, B. T. Matthias, T. H. Geballe, and E. Corenzwit, Phys. Rev. Lett. **8**, 408 (1962).

[17] B. T. Matthias, T. H. Geballe, and V. B. Compton, Mod. Phys. **35**, 414 (1963).

[18] P. Blaha, K. Schwarz, G. Madsen, D. Kvasnicka and J. Luitz, WIEN2k, An Augmented Plane Wave + Local Orbitals Program for calculating Crystal Properties, Technische Universitat Wien, Austria, (2001).

[19] D. J. Singh, L. Nordstrom, Planewaves, Pseudopotentials, and the LAPW Method, Springer, New York, 2^{nd} ed. (1996).

[20] G. K. H. Madsen, P. Blaha, K. Schwarz, E. Sjostedt, L. Nordstrom, Efficient linearization of the augmented plane-wave method, Phys. Rev. B 64 **19**, 195134 (2001).

[21] E. Sjostedt, L. Nordstrom, D. J. Singh, An alternative way of linearizing the augmented plane-wave method, Solid State Communications **114**15-20 (2000).

[22] J. P. Perdew, K. Burke and M. Ernzerhof, Phys Rev Lett. **77**, 3865 (1996).

[23] M. Tinkham, Introduction to Superconductivity, 2nd ed. McGraw Hill, New York (1975).

[24] A. F. Ioffe and A. R. Regel, Prog. Semicond. **4**, 237 (1961).

[25] V. N. Zverev, A. V. Korobenko, G. L. Sun, D. L. Sun, C. T. Lin, and A. V. Boris, JETP Lett. **90**, 130 (2009).

[26] Charles Kittel, Introduction to Solid State Physics, Seventh Edition, John Wiley and Sons, Inc. New York (1996).

[27] A. B. Karki, Y. M. Xiong, I. Vekhter, D. Browne, P. W. Adams, K. R. Thomas, H. Kim, R. Prozorov, Julia Y. Chan and D. P. Young, Phys. Rev. B **82**, 064512 (2010).

[28] A. B. Karki, Y. M. Xiong, N. Haldolaarachchige, W. A. Phelan, Julia Y. Chan, S. Stadler, I. Vekhter, P. W. Adams, and D. P. Young, Phy. Rev. B, **83**, 144525 (2011).

[29] Neel Haldolaarachchige, Quinn Gibson, Jason Krizan, and R. J. Cava, Phy. Rev. B **89**, 104520 (2014).

[30] Mazhar N. Ali, Quinn D. Gibson, T. Klimczuk, and R. J. Cava, Physical Review B **89**, 020505(R) (2014).

[31] Huixia Luo, Tomasz Klimczuk, Lukas Muchler, Leslie Schoop, Daigorou Hirai, M. K. Fuccillo, C. Felser, and R. J. Cava Physical Review B **87**, 214510 (2013).

[32] M. D. Lan, J. C. Chang, K. T. Lu, C. Y. Lee, H. Y. Shih, and G. Y. Jeng, IEEE Transaction on Applied Superconductivity, **11**, 3607-3610 (2001).

[33] Leslie M. Schoop,1, Lilia S. Xie,1 Ru Chen, Quinn D. Gibson, Saul H. Lapidus, Itamar Kimchi, Max Hirschberger, Neel Haldolaarachchige, Mazhar N. Ali, Carina A. Belvin, Tian Liang, Jeffrey B. Neaton, N. P. Ong, Ashvin Vishwanath, and R. J. Cava, Phy. Rev. B **91**, 214517 (2015).

[34] Neel Haldolaarachchige, Satya Kushwaha, Quinn Gibson and R. J. Cava, Sup. Cond. Sci. and Tech. **27**, 105001 (2014).

[35] N. R. Werthamer, E. Helfand and P. C. Hohenberg, Phys. Rev. **147**, 295 (1966).

[36] A. M. Clogston, Phys. Rev. Lett. **09**, 266 (1962).

[37] H. Padamsee, J. E. Neighbor, and C. A. Shiffman, J. Low Temp. Phys. **12**, 387 (1973).

[38] W. L. McMillan, Phys. Rev. **167**, 331 (1968).

[39] Handbook of Superconductivity, edited by C. P. Poole Jr. (Academic Press, New York, 1999), Chap. 9, Sec. G, p. 478.

[40] A. C. Jacko, J. O. Fjaerestad and B. J. Powell, Nature Physics **5**, 422 (2009).

[41] K. G. Wilson, Rev. Mod. Phys. **47**, 773 (1975).

[42] K. Yamada, Prog. Theor. Phys. **53**, 970 (1975).